Myogenic contractions of a somatic muscle powers rhythmic flow of hemolymph through *Drosophila* antennae and generates brain pulsations

Alan R. Kay[1*], Daniel F. Eberl[1] and Jing W. Wang[2]

[1]Dept. Biology, University of Iowa, Iowa City, IA 52242 and [2]Neurobiology Section, Division of Biological Sciences, University of California, San Diego, CA 92093.

*Author for correspondence (alan-kay@uiowa.edu)

Abbreviations:
a1, a2 & a3 – first, second & third antennal segments
AM - ampullary membrane
AV - antennal vessel
FPO -frontal pulsatile organ
m16 – muscle 16

ABSTRACT
Hemolymph is driven through the antennae of *Drosophila melanogaster* by the rhythmic contraction of muscle 16 (m16), which runs through the brain. Contraction of m16 results in the expansion of an elastic ampulla, opening ostia and filling the ampulla. Relaxation of the ampullary membrane forces hemolymph through vessels into the antennae. We show that m16 is an auto-active rhythmic somatic muscle. The activity of m16 leads to the rapid perfusion of the antenna by hemolymph. In addition, it leads to the rhythmic agitation of the brain, which could be important for clearing the interstitial space.

KEY WORDS: antenna, *Drosophila*, heart, myogenic, pulsatility, somatic muscle

Summary statement
The circulation of hemolymph in the antenna of *Drosophila* is powered by the rhythmic contraction of an auto-active somatic muscle which runs through the brain.

INTRODUCTION

The slowness of diffusion over distances of more than about 10 μm serves as a spur for the evolution of active circulatory systems (Berg, 1993). The flow of hemolymph in insects is driven by contraction of the dorsal vessel (heart) in the abdomen, which propels hemolymph into the non-contractile dorsal aorta in the thorax (Hillyer and Pass, 2020; Rotstein and Paululat, 2016). From here the hemolymph flows into the head cavity and then back into the hemocoel of the thorax and abdomen, where it is actively drawn into the heart. This flow of hemolymph is adequate for the body but insufficient to drive hemolymph into small appendages like the legs, wings, cerci and antennae. Flow into these structures is driven by accessory pulsatile organs that operate independently of the heart (Pass, 2000).

There are a number of different anatomical arrangements that drive circulation through the antenna (Pass, 2000). In Diptera, a muscle (m16) that extends through the brain is attached to an ampulla, which together constitute the frontal pulsatile organ (FPO)(Miller, 1950). In other insects this organ is referred to as the 'antennal accessory pulsatile organ' or 'antennal heart' (Pass, 2000).

Journal of Experimental Biology • Accepted manuscript

The ampulla is located medially behind the prefrons and ventral to the ptilinal fold (Miller, 1950). Contraction of m16 stretches an elastic ampullary membrane (AM) on the caudal side of the ampulla, which opens valves (ostia) that allow the influx of hemolymph into the ampulla (Fig. 1 B&C). When m16 relaxes, the tension developed in the AM leads to an elevation of pressure, closing the ostia and forcing the hemolymph into the antennal vessels, which carry the fluid through the first antennal segment (a1), the second antennal segment (a2) and then through the stalk into the third antennal segment (a3) (Fig. 1 A). Flow through the antenna is driven by a passive systole since it does not rely on direct muscular contraction, rather the relaxation of a stretched elastic compartment.

Here we characterize the structure and physiology of the FPO in *Drosophila melanogaster*. The pulsing of the FPO has been noted in *Drosophila*, where its action interferes with electrophysiological recordings (Murthy and Turner, 2010) and the rudiments of its anatomy have been described (Miller, 1950). It is by no means obvious that *Drosophila*, with small antennae, needs to circulate hemolymph actively; and flow through the antennae has not been previously demonstrated in *Drosophila*.

Although the hearts of insects and vertebrates are morphologically quite distinct, it is striking that the homologous transcription factor *tinman* determines the cardiac cell lineage in both *Drosophila* and vertebrates (Bodmer, 1993; Burkhard et al., 2017). It is worth noting that all three classes of muscle (somatic, cardiac and visceral) in *Drosophila* are striated (Taylor, 2006) unlike vertebrates, which have unstriated smooth muscle.

MATERIALS AND METHODS

Fly stocks

Experiments were performed on adult flies of the following strains:
Control flies were from the Canton S strain.
The following strains from the Bloomington *Drosophila* Stock Center were used:
elav^{C155}-Gal4 UAS-mCD8-GFP strain (Bloomington *Drosophila* Stock Center stock #5146), with the following genotype: *P{w$^{+mW.hs}$=GawB}elav^{C155}, P{w^{+mC}=UAS-mCD8::GFP.L}Ptp4E^{LLA}, P{ry$^{+t7.2}$=hsFLP}1, w*.*
Mhc-Tau-GFP strain, (stock #38460) of genotype: *w*; P{w^{+mC}=Act88F-GAL4.1.3}81B, P{w^{+mC}=Mhc-tauGFP}2/SM6b*
Trachea marker strain (stock # 41803), genotype: *y^{1} w*; wg^{Sp-1}/CyO; P{w^{+mC}=btl-moe.mRFP1}3, P{w^{+mC}=GAL4-btl.S}3-1, P{w^{+mC}=UAS-mCD8::GFP.L}LL6/TM6B, Tb^{1}.*

Gal4 driver lines that express in heart included the following two strains:
w; tinCD4-Gal4 (Lo and Frasch, 2001)
y w; hand$^{4.2}$-Gal4 (Han and Olson, 2005)

Physiological experiments

Flies were cold-anesthetized for about one minute, by introducing them into a small glass test tube held on ice. For intact fly experiments, anesthetized flies were affixed to a coverslip by a small droplet of light cured resin. To open the head, the goggatomy procedure of Kay et al. (2016) was employed. In brief, a cold anesthetized fly was decapitated, and the head placed in a drop of resin. After curing for 1 min, a drop of saline was placed over the cured specimen, which was then cut by hand with a carbon steel blade (Feather Safety Razor Co., Japan). The section was then mounted on a piece of wax melted on to the floor of a chamber (Siskiyou Corp., Grants Pass, OR) filled with saline. The composition of the saline in (mM): 120 NaCl, 3 mM KCl, 1 $CaCl_2$, 4 $MgCl_2$, 4 NaHCO3, 1 NaH_2PO_4, 8 D-trehalose, 5 D-glucose and 5 TES (pH 7.2). The bath solution was stirred with a stream of air from a fish tank pump.

Whole flies or sectioned preparations were imaged on an Olympus BX50WI upright microscope equipped with a Hamamatsu ORCA-Flash 4.0 CMOS camera. Illumination was provided by an X-Cite 120 LED (Excelitas Technologies Corp., Waltham, MA) through a Semrock (Rochester, NY) BrightLine filter set (472/30 Bandpass, 495 Dichroic and a 520/35 Bandpass) and controlled by MetaMorph software (Molecular Devices, Sunnyvale, CA).

Measuring hemolymph flow

To monitor the flow of hemolymph, cold-anesthetized flies were injected with saline containing 0.5 µm diameter fluorescent beads (carboxyl-functionalized microspheres, Dragon Green (Bangs Beads, Fishers, IN)), diluted 1/20 v/v. A glass microelectrode with a tip diameter of approximately 10 µm was used to inject ~ 30 nL into the thorax of a fly that had been secured to a glass cover slip with light-cured resin. Movement of the beads was imaged through the cuticle and was analyzed using ImageJ (Rueden et al., 2017).

Histology

The heads of cold-anesthetized flies were fixed in 2% glutaraldehyde in PBS with 4 mM $MgCl_2$ for 24 hours at 4°C. Prior to placing the head in fixative, the tip of the proboscis was cut off to allow better penetration of the fixative. The heads were then dehydrated in graded ethanol and propylene oxide, embedded with Epon 812 in beam capsules and polymerized at 60 °C for at least 24 h. Sections were cut using a Leica RM2265 rotary microtome and stained with Azure-methylene blue (Richardson et al., 1960). Images were acquired by QImaging 5.0 RTV camera mounted on a Nikon E800.

Data is presented as average ± SD. Graphs were produced using Origin (OriginLab Corp, Northampton, MA). All chemicals, unless otherwise noted, were from Millipore-Sigma.

RESULTS

Anatomy of the FPO

The structure of the components of the FPO was examined in serial sections using light microscopy (Fig. 2). The ampulla is bounded on its posterior end by an AM, which is composed of thin nucleated cells. The ampulla is empty except for what appear to be fat cells opposed to the cuticular side of the structure. In live flies injected with fluorescent beads, we detected the influx of beads into the ampulla through ostia in the AM (see below). However, the ostia were not evident in serial sections; this is likely so because the AM is fixed in its relaxed form when the ostial flaps are closed and are hence difficult to detect.

Bilateral antennal vessels (AVs) emerge from the sides of the ampulla and pass into a1. Within a2 the AV enters the stalk of the a2-a3 joint, and passes into a3. The AV runs along the lateral edge of a3, sending a collateral branch to the arista (Foelix et al., 1989) and terminates as a funnel about three quarters of the way down a3.

The FPO dilator muscle, m16 is composed of two muscles, each with two to three fibers, attached to the AM. The muscles course together, directly through the medial canal in the brain. The muscles have a clearly striated appearance and are fluorescent in the *Mhc-tau-GFP* flies, in which somatic muscle is labeled (Weitkunat and Schnorrer, 2014). At its posterior end within the medial canal, the two strands of m16 run in very close apposition and are attached via - what appears to be - a ligament to the glial sheath surrounding the brain and to tracheal air sacs on the posterior surface of the brain. The ligaments are not connected directly to the head cuticle. Within the median canal, m16 runs dorsal to and in close contact with the esophagus.

It is worth noting that the antennal circulation does not receive hemolymph directly from the aorta, since the inflow to the ampulla is located anterior to the brain, while the aorta ends posterior to the brain as the aortic funnel (Miller, 1950)(Fig. 2B). Hemolymph entering the head capsule from the aorta flows over the brain to reach the ostia of the ampulla.

To identify the lineage of m16 we used several *Drosophila* strains expressing GFP under the control of a variety of regulatory elements. M16 was not labeled by *hand-c (Sellin et al., 2006)*, which demarcates muscles in the dorsal heart and wing hearts, nor by *tinman,* which defines cells in the cardiac lineage (Zaffran et al., 2006).

We were unable to detect nerves innervating m16 in histological sections or in goggatomized sections of flies expressing GFP pan-neuronally. However, others have identified an octopaminergic input onto m16 (Pauls et al., 2018). In cockroaches, modulatory nerves are found connected to the muscle (Pass et al., 1998).

Non-invasive detection of FPO activity

The activity of m16 can be observed in intact flies using bright field imaging through the cuticle or in flies expressing fluorescent proteins. Beating of the FPO can be detected through the prefrons in live flies, by affixing the anterior surface of the fly's head to a coverslip with light-cured resin. The movement of the AM below the cuticle of the prefrons can be seen in bright field videos (Fig. 3A).

In flies where muscles were labelled with GFP linked to *Mhc-Tau*, m16 could be imaged through the head capsule when the flies were fixed to a glass coverslip. As m16 rhythmically contracts, the anterior end of the muscle moves in and out of the plane of focus (Fig. 3 B)

When the m16 and the aristae were imaged simultaneously, both antennae moved in synchrony with the beating of m16 (Fig. 3c). In addition, the esophagus which runs in very close proximity to m16 moves in concert with m16 ((Figure S1).

Since m16 passes through the median canal in the brain and is attached to the posterior aspect of the brain, contraction results in movement of the brain. This can be seen in flies expressing a pan neuronal GFP (elav-GFP). If one focuses on any part of the brain the fluorescent intensity oscillates at the same rate as the m16 (Fig. 3 d). Movement of the thoracic ganglion was also noted but is synchronized with the abdominal heart,), which is not in synchrony with the FPO (Figure S2) .

In a fly line where the tracheae are labeled with GFP, brain movement driven by the m16 could be detected, superimposed on movement driven by respiration (Figure S3).

M16 activity in an exposed preparation

We have used the goggatomy procedure (Kay et al., 2016) to cut sections through the head, while preserving an intact beating m16, to expose and view m16 directly. In this experiment, the head was cut transversely parallel to a line through the a2-a3 junctions, and the dorsal half of the head observed. In many cases m16 survived the procedure and could be seen beating, pulling on the AM and the brain (Movie 1). In all cases the contraction of both muscles was coordinated. Beating goggotamized preparations routinely survived for six hours, however all experiments reported here were performed within one hour of sectioning the head.

We tested whether the application of TTX had an effect on the beating frequency of m16 in goggotamized preparations (Mhc-tau-GFP). The mean frequency before application of TTX was 1.72 ± 0.42 Hz, while 5 min after application of TTX (5 μm), the mean frequency was 1.67 ± 0.29 Hz, not significantly different (2-tailed paired t-test, $p = 0.489$, $N = 14$). This suggests that the rhythm is myogenic and that TTX-sensitive sodium channels do not play a role in the pacemaker mechanism. Beating of m16 was observed whether the head was cut dorsal or ventral to m16. This

also argues against a motoneuron driving contractions, since one of the cuts would be expected to section the nerve.

The mechanism for generating the rhythmic myogenic activity could be entirely contained within the muscle cells, much like the pacemaker cells of the sino-atrial node where an ensemble of voltage-gated channels generates the regular rhythmic activity (Boron and Boulpaep, 2016; Burkhard et al., 2017). It is also possible that the mechanical tension on m16 could drive pacing. However, detaching the posterior connection of the m16 did not stop the pulsing of the muscle, arguing against this scenario (Figure S4).

Superfusing the muscle with saline with no added calcium and 1mM EGTA (+4mM $MgCl_2$) led to contractions ceasing within a few seconds. If the EGTA was omitted, m16 remained rhythmic for 10-20 min. It then entered a period of irregular beating before ceasing. At all times both muscles beat at the same irregular frequency. The fact that the removal of calcium did not halt beating immediately is further evidence that the rhythm is not neurogenic.

As the solution was changed from zero Ca^{2+} to normal saline and vice versa, there were periods where propagating waves of contraction were observed in m16 (data not shown). These were observed to occur independently in the left and right m16 muscles. This points to Ca^{2+} -induced-Ca^{2+} release within the myoplasm.

Flow Rate

To monitor the flow of hemolymph through the antennae, fluorescent beads (Boppana and Hillyer, 2014) were injected into the thorax while the head of the fly was attached to a cover slip with light-cured resin. The flow of beads was then observed using fast epi-fluorescent imaging.

Flow of beads could be detected into and out of the ampulla when imaged through the prefrons. During diastole, beads could be seen flowing in through ostia in the ventral portion of the AM, while during systole, the beads were ejected into the bilateral AVs (Fig. 5).

The passage of beads could be followed through the antennae, moving within the AV that courses through a1, then a2 and terminates in a3. At the latter site, hemolymph flows into the interior of a3, then through the stalk into a2, a1, and into the head cavity.

Kymograph plots were used to visualize and quantify the flow of beads in the AV and a3. To transform a video into a kymograph plot, a straight line is drawn along the flow of beads through the AV. For the first video frame the intensity along this line is drawn parallel to the y-axis of a 2D plot. For the next frame the intensity along the line is placed just to the right of the last line. Repeating this procedure generates the kymograph with the x-axis representing time. A bead moving at uniform velocity traces a straight line on a kymograph, with the slope of the line equal to the velocity. It was also possible to visualize directly, in some cases, the beating of the FPO as well as the passage of beads through the antenna (Fig. 8). If one plots the activity of the FPO (blue trace Fig. 8) alongside kymographs, one can see that bead flow accelerates during systole (blue trace up) and decelerates during diastole (blue trace down). In the example shown in fig. 8, the peak flow velocity during systole in the AV was 178.6 ± 44.4 um/s, while for the dorsally directed flow in a3 it was 33.8 ± 7.3 um/s (n=14). This is consistent with a larger cross-sectional area in the return flow pathway compared to the AV. The minimum flow velocity during the diastole in the AV was 4.1 ± 1.1 um/s, and for the dorsally directed flow 0.7 ± 0.3 um/s (n=14).

We were also able to detect flow of beads into and out of the base of the arista, from a tributary of the AV (data not shown)

DISCUSSION

The circulation of hemolymph through the antenna is driven by the pulsatile stretching of the elastic AM by m16. Unlike the dorsal heart, which reverses flow periodically (Wasserthal, 2007), beating of the m16 is constant and proceeds without abate. Unusually, although m16 is involved in circulation, it is a somatic muscle, that appears to be outside of the cardiac lineage and its rhythmicity is myogenic. Myogenic antennal hearts have been described in cockroaches (Hertel et al., 1985) and mosquito (Boppana and Hillyer, 2014).

M16 is attached to the flexible membrane of the ampulla, however the nature of this membrane and the attachments are unknown. The AM does not appear to contain resilin, since it is not UV fluorescent (Andersen and Weis-Fogh, 1964). m16 is attached at its posterior end by ligaments to air sacs, the sheath surrounding the brain and the aortic funnel. Hence contraction of m16 pulls the brain in an anterior direction. It is possible that this motion serves to inflate and deflate the air sacs and to agitate the hemolymph in the head capsule, facilitating its dispersal.

Additional functions of the FPO

The flow of hemolymph in insects serves to circulate ions, nutrients, hormones and waste products, but only to a small extent oxygen, which is primarily carried by the tracheal system (Chapman et al., 2012). At simplest, the FPO circulates hemolymph through a restricted space that is cut off from the general flow of hemolymph through the hemocoel. As with any physiological system, the functions of the FPO are likely to be diverse. Consequently, it is worth enquiring whether the function of the FPO extends beyond simply circulating hemolymph through the antennae. Other possible functions for the FPO are:

a) The FPO may act as a neurohaemal organ, as it does in cockroaches (Pass et al., 1988). Rapid flow may be used to quickly change the hormones supplied to the olfactory receptor neurons and scolopidia.
b) The pressure generated by the FPO may be necessary to prevent the antennae from collapsing and to keep them erect.
c) The rapid circulation may be necessary to refresh the intra-antennal hemolymph sweeping away odorant molecules that might accumulate.
d) The olfactory receptor neurons and scolopidia in Johnston's organ might have a very high rate of metabolism and require vigorous delivery of glucose and other nutrients.
e) The pulsatility of the brain induced by action of the FPO may be necessary for normal function. We will expand on this below.

In what is probably its ancestral/primitive form, as in cockroaches, the FPO comprises two bilateral ampulla that serve each antenna separately (Pass, 2000). The homolog of m16 extends across the head capsule connecting to the two ampullae. It is interesting that in cockroaches there is a smaller muscle that attaches to the middle of m16 and extends through the brain. It seems likely that during evolution the ampullae fused in *Drosophila*. It is possible that the FPO in *Drosophila* is an evolutionary remnant from ancestors that had far longer antennae (Pass et al., 2006) and required a vigorous antennal circulation.

m16 is a myogenic pacemaker

M16 is an interesting case of an auto-active somatic muscle functioning as a heart. M16 does not appear to be part of the cardiac lineage. Like the sino-atrial node (Monfredi et al., 2010) of vertebrate hearts, m16 appears to be a myogenic pacemaker. And, like the former, it has a complement of ion channels that endows it with these properties. There are two m16s side by side, each with a few separate strands, all contracting in synchrony. Detaching the caudal attachment of m16 muscle did not lead to a loss of synchrony, suggesting that the muscle strands are not mechanically coupled. It seems likely that the muscles are coupled by gap junctions. Our evidence for

electrical coupling is that TTX does not block the rhythmic activity of the FPO, consistent with a myogenic rather than neurogenic pacemaker. Moreover, in a few cases where m16 was beating irregularly, both strands remained coordinated. If the strands were not electrically coupled, they would be expected to contract independently.

There appear to be myogenic pacemakers in both the larval and adult dorsal hearts, as in both cases TTX is ineffective in halting the rhythmic contraction (Gu and Singh, 1995; Johnson et al., 1998). However, in both cases the location and precise nature of the pacemakers is unknown. The adult heart regularly alternates periods of anterograde and retrograde beating (Wasserthal, 2007); the switching of the direction of flow is centrally controlled (Dulcis and Levine, 2005). As in other insect hearts, myotropic neuropeptides may alter the pacing of m16 (Suggs et al., 2016).

It is worth pointing out that the goggatomized head preparation, with the intact beating FPO, could serve as a simple, cost effective laboratory preparation to use in teaching laboratories to illustrate the operation of myogenic pacemakers.

CNS pulsatility

Action of the m16 drives pulsation of the fly brain. This has previously been observed by others (Murthy and Turner, 2010; Paulk et al., 2013). Brain movement has been measured with a displacement sensor in blowflies (Vahasoyrinki et al., 2009), where periodic excursions occur of up to 5 μm.

Vertebrate brains experience a similar pulsatility since they are coupled to a rhythmic heart. Pressure waves couple through to the parenchyma and give rise to small transient periodic changes in pressure accompanied by small displacements (Mosher et al., 2020). It has been argued that this pulsatility is necessary for brain vitality, since holding the pulsatility in abeyance, as occurs in cardiac bypass surgery, may lead to a decline in cognitive function (so-called pumphead) (Mark and Newman, 2002; O'Neil et al., 2012; Stutz, 2009). Interrupting pulsatility in experiments on piglets led to a decline in the condition of the tissue as judged by the levels of ATP. (O'Neil et al., 2012; Salameh et al., 2015).

We suggest that the movement of the fly brain might serve to aid in removing metabolic waste products from the extracellular space that accumulate because of neural activity. A similar mechanism has been proposed to drain extracellular fluid in the mammalian brains along perivascular spaces (Iliff et al., 2013; Sharp et al., 2016; van Veluw et al., 2019) in the so-called glymphatic system (Mestre et al., 2020). It could also be that movement of the brain induces deformation of the very fine tracheoles that penetrate the brain and aid gas exchange.

JO Pulsatility

The a2 contains Johnston's organ, which is a fan-like array of chordotonal organs that are very sensitive to rotation of a3 about the axis of the stalk which connects a2 to a3 (Eberl et al., 2016). Near-field sound impinging on the arista drives the motion of this joint. It has been estimated that the JO is sensitive to linear stretches of the chordotonal organs of less than 1 nm (Robert and Göpfert, 2002). However, the organ is not static and exhibits oscillatory behavior that is believed to arise from intrinsic vibrations of the scolopidia at a frequency close to 200 Hz (Göpfert et al., 2005; Göpfert and Robert, 2003). These oscillations improve the sensitivity of the JO. This is 2 orders of magnitude higher frequency than the FPO rate, so the JO-derived spontaneous oscillations of the arista are superimposed on the much slower FPO oscillations. In this study, we have found that the arista vibrates in concert with the action of the FPO. If the fly is to reliably detect sound, gravity or wingbeat amplitude (Mamiya et al., 2011) it seems likely that it has a mechanism for compensating for the self-motion of the arista. m16 runs in close proximity to the brain, all that is required is a mechanosensor located within the brain to pick up its action.

In conclusion, m16 could serve as a very useful model for the sino-atrial node pacemaker since it is a circumscribed and easily accessible system, while the pacemaker cells in the dorsal heart of *Drosophila* have not been located. Moreover, m16 in *Drosophila* could also serve as a model system for exploring the effects of pulsatility on brain function.

Acknowledgments
We thank Jennifer Kersigo for advice on preparing histological sections, Grace Boekhoff-Falk and Lori Wallrath for providing fly stocks, and David Kleinfeld, Bridget Lear and Bernd Fritzsch for the loan of equipment.

Competing interests: The authors declare no competing or financial interests.

Author contributions: Author contributions Conceptualization: A.R.K..; Methodology: A.R.K., D.F.E. & J.W.W.; Validation: A.R.K.; Formal analysis: A.R.K.; Investigation: A.R.K.*; Resources*: A.R.K., D.F.E, &J.W.; Writing - original draft: A.R.K.; Writing - review & editing: A.R.K., D.F.E, & J.W.W.; Visualization: A.R.K.; Supervision: A.R.K.; Funding acquisition: J.W.W.

Funding
This work was partially supported by an NIH grant to J.W.W. (R01DK092640) and an NSF grant to A.R.K and D.F.E (2037828).

Data availability

Supplementary information: Supplementary information available online at ……..

References

Andersen, S. O. and Weis-Fogh, T. (1964). Resilin. A rubberlike protein in arthropod cuticle. In *Advances in Insect Physiology*, vol. 2, pp. 1-65: Elsevier.

Berg, H. C. (1993). Random Walks in Biology. Princeton, NJ: Princeton University Press.

Bodmer, R. (1993). The gene tinman is required for specification of the heart and visceral muscles in Drosophila. *Development* **118**, 719-729.

Boppana, S. and Hillyer, J. F. (2014). Hemolymph circulation in insect sensory appendages: functional mechanics of antennal accessory pulsatile organs (auxiliary hearts) in the mosquito Anopheles gambiae. *J Exp Biol* **217**, 3006-14.

Boron, W. F. and Boulpaep, E. L. (2016). Medical Physiology: A cellular and molecular approach: Elsevier.

Burkhard, S., Van Eif, V., Garric, L., Christoffels, V. M. and Bakkers, J. (2017). On the evolution of the cardiac pacemaker. *Journal of cardiovascular development and disease* **4**, 4.

Chapman, R. F., Simpson, S. J. and Douglas, A. E. (2012). The Insects: Structure and fFunction: Cambridge University Press.

Dulcis, D. and Levine, R. B. (2005). Glutamatergic innervation of the heart initiates retrograde contractions in adult Drosophila melanogaster. *Journal of Neuroscience* **25**, 271-280.

Eberl, D. F., Kamikouchi, A. and Albert, J. T. (2016). Auditory Transduction. In *Insect Hearing*, pp. 159-175: Springer.

Foelix, R. F., Stocker, R. F. and Steinbrecht, R. A. (1989). Fine structure of a sensory organ in the arista of Drosophila melanogaster and some other dipterans. *Cell Tissue Res* **258**, 277-87.

Göpfert, M. C., Humphris, A. D. L., Albert, J. T., Robert, D. and Hendrich, O. (2005). Power gain exhibited by motile mechanosensory neurons in Drosophila ears. *Proceedings of the National Academy of Sciences of the United States of America* **102**, 325-30.

Göpfert, M. C. and Robert, D. (2003). Motion generation by Drosophila mechanosensory neurons. *Proceedings of the National Academy of Sciences of the United States of America* **100**, 5514-9.

Gu, G. G. and Singh, S. (1995). Pharmacological analysis of heartbeat in Drosophila. *Journal of Neurobiology* **28**, 269-280.

Han, Z. and Olson, E. N. (2005). Hand is a direct target of Tinman and GATA factors during Drosophila cardiogenesis and hematopoiesis. *Development* **132**, 3525-3536.

Hertel, W., Pass, G. and Penzlin, H. (1985). Electrophysiological investigation of the antennal heart of Periplaneta americana and its reactions to proctolin. *Journal of insect physiology* **31**, 563-572.

Hillyer, J. F. and Pass, G. (2020). The Insect Circulatory System: Structure, Function, and Evolution. *Annual review of entomology* **65**, 121-143.

Iliff, J. J., Wang, M., Zeppenfeld, D. M., Venkataraman, A., Plog, B. A., Liao, Y., Deane, R. and Nedergaard, M. (2013). Cerebral arterial pulsation drives paravascular CSF-interstitial fluid exchange in the murine brain. *J Neurosci* **33**, 18190-9.

Johnson, E., Ringo, J., Bray, N. and Dowse, H. (1998). Genetic and pharmacological identification of ion channels central to the Drosophila cardiac pacemaker. *Journal of neurogenetics* **12**, 1-24.

Kay, A. R., Raccuglia, D., Scholte, J., Sivan-Loukianova, E., Barwacz, C. A., Armstrong, S. R., Guymon, C. A., Nitabach, M. N. and Eberl, D. F. (2016). Goggatomy: A Method for Opening Small Cuticular Compartments in Arthropods for Physiological Experiments. *Front Physiol* **7**, 398.

Lo, P. C. and Frasch, M. (2001). A role for the COUP-TF-related gene seven-up in the diversification of cardioblast identities in the dorsal vessel of Drosophila. *Mechanisms of development* **104**, 49-60.

Mamiya, A., Straw, A. D., Tómasson, E. and Dickinson, M. H. (2011). Active and passive antennal movements during visually guided steering in flying Drosophila. *J Neurosci* **31**, 6900-14.

Mark, D. B. and Newman, M. F. (2002). Protecting the brain in coronary artery bypass graft surgery. *JAMA* **287**, 1448-1450.

Mestre, H., Mori, Y. and Nedergaard, M. (2020). The Brain's Glymphatic System: Current Controversies. *Trends in Neurosciences*.

Miller, A. (1950). The internal anatomy and histology of the imago of Drosophila melanogaster. New York, NY: John Wiley & Sons, Inc.

Monfredi, O., Dobrzynski, H., Mondal, T., Boyett, M. R. and Morris, G. M. (2010). The anatomy and physiology of the sinoatrial node—a contemporary review. *Pacing and clinical electrophysiology* **33**, 1392-1406.

Mosher, C. P., Wei, Y., Kaminski, J., Nandi, A., Mamelak, A. N., Anastassiou, C. A. and Rutishauser, U. (2020). Cellular Classes in the Human Brain Revealed In Vivo by Heartbeat-Related Modulation of the Extracellular Action Potential Waveform. *Cell Rep* **30**, 3536-3551 e6.

Murthy, M. and Turner, G. (2010). In vivo whole-cell recordings in the *Drosophila* brain. In *Drosophila Neurobiology: A laboratory manual*, eds. B. Zhang M. R. Freeman and S. Waddell), pp. 534. New York: Cold Spring Harbor Laboratory Press.

O'Neil, M. P., Fleming, J. C., Badhwar, A. and Guo, L. R. (2012). Pulsatile versus nonpulsatile flow during cardiopulmonary bypass: microcirculatory and systemic effects. *Ann Thorac Surg* **94**, 2046-53.

Pass, G. (2000). Accessory pulsatile organs: evolutionary innovations in insects. *Annu Rev Entomol* **45**, 495-518.

Pass, G., Agricola, H., Birkenbeil, H. and Penzlin, H. (1988). Morphology of neurones associated with the antennal heart of Periplaneta americana (Blattodea, Insecta). *Cell Tissue Res* **253**, 319-26.

Pass, G., Gereben-Krenn, B.-A., Merl, M., Plant, J., Szucsich, N. U. and Tögel, M. (2006). Phylogenetic relationships of the orders of Hexapoda: contributions from the circulatory organs for a morphological data matrix. *Arthropod Syst. Phylogeny* **64**, 165-203.

Pass, G., Sperk, G., Agricola, H., Baumann, E. and Penzlin, H. (1998). Octopamine in a neurohaemal area within the antennal heart of the American cockroach. *Journal of Experimental Biology* **135**, 495-498.

Paulk, A. C., Zhou, Y., Stratton, P., Liu, L. and van Swinderen, B. (2013). Multichannel brain recordings in behaving Drosophila reveal oscillatory activity and local coherence in response to sensory stimulation and circuit activation. *J Neurophysiol* **110**, 1703-21.

Pauls, D., Blechschmidt, C., Frantzmann, F., el Jundi, B. and Selcho, M. (2018). A comprehensive anatomical map of the peripheral octopaminergic/tyraminergic system of Drosophila melanogaster. *Sci Rep* **8**, 1-12.

Richardson, K., Jarett, L. and Finke, E. (1960). Embedding in epoxy resins for ultrathin sectioning in electron microscopy. *Stain technology* **35**, 313-323.

Robert, D. and Göpfert, M. C. (2002). Novel schemes for hearing and orientation in insects. *Current Opinion in Neurobiology* **12**, 715-720.

Rotstein, B. and Paululat, A. (2016). On the morphology of the Drosophila heart. *Journal of cardiovascular development and disease* **3**, 15.

Rueden, C. T., Schindelin, J., Hiner, M. C., DeZonia, B. E., Walter, A. E., Arena, E. T. and Eliceiri, K. W. (2017). ImageJ2: ImageJ for the next generation of scientific image data. *BMC Bioinformatics* **18**, 529.

Salameh, A., Kuhne, L., Grassl, M., Gerdom, M., von Salisch, S., Vollroth, M., Bakhtiary, F., Mohr, F. W., Dahnert, I. and Dhein, S. (2015). Protective effects of pulsatile flow during cardiopulmonary bypass. *Ann Thorac Surg* **99**, 192-9.

Sellin, J., Albrecht, S., Kölsch, V. and Paululat, A. (2006). Dynamics of heart differentiation, visualized utilizing heart enhancer elements of the Drosophila melanogaster bHLH transcription factor Hand. *Gene Expression Patterns* **6**, 360-375.

Sharp, M. K., Diem, A. K., Weller, R. O. and Carare, R. O. (2016). Peristalsis with Oscillating Flow Resistance: A Mechanism for Periarterial Clearance of Amyloid Beta from the Brain. *Ann Biomed Eng* **44**, 1553-65.

Stutz, B. (2009). Pumphead: Does the heart-lung machine have a dark side? *Scientific American*.

Suggs, J. M., Jones, T. H., Murphree, S. C. and Hillyer, J. F. (2016). CCAP and FMRFamide-like peptides accelerate the contraction rate of the antennal accessory pulsatile organs (auxiliary hearts) of mosquitoes. *J Exp Biol* **219**, 2388-95.

Taylor, M. V. (2006). Comparison of muscle development in Drosophila and vertebrates. In *Muscle Development in Drosophila*, pp. 169-203: Springer.

Vahasoyrinki, M., Tuukkanen, T., Sorvoja, H. and Pudas, M. (2009). A minimally invasive displacement sensor for measuring brain micromotion in 3D with nanometer scale resolution. *J Neurosci Methods* **180**, 290-5.

van Veluw, S. J., Hou, S. S., Calvo-Rodriguez, M., Arbel-Ornath, M., Snyder, A. C., Frosch, M. P., Greenberg, S. M. and Bacskai, B. J. (2019). Vasomotion as a Driving Force for Paravascular Clearance in the Awake Mouse Brain. *Neuron*.

Wasserthal, L. T. (2007). Drosophila flies combine periodic heartbeat reversal with a circulation in the anterior body mediated by a newly discovered anterior pair of ostial valves and 'venous' channels. *J Exp Biol* **210**, 3707-19.

Weitkunat, M. and Schnorrer, F. (2014). A guide to study Drosophila muscle biology. *Methods* **68**, 2-14.

Zaffran, S., Reim, I., Qian, L., Lo, P. C., Bodmer, R. and Frasch, M. (2006). Cardioblast-intrinsic Tinman activity controls proper diversification and differentiation of myocardial cells in Drosophila. *Development* **133**, 4073-4083.

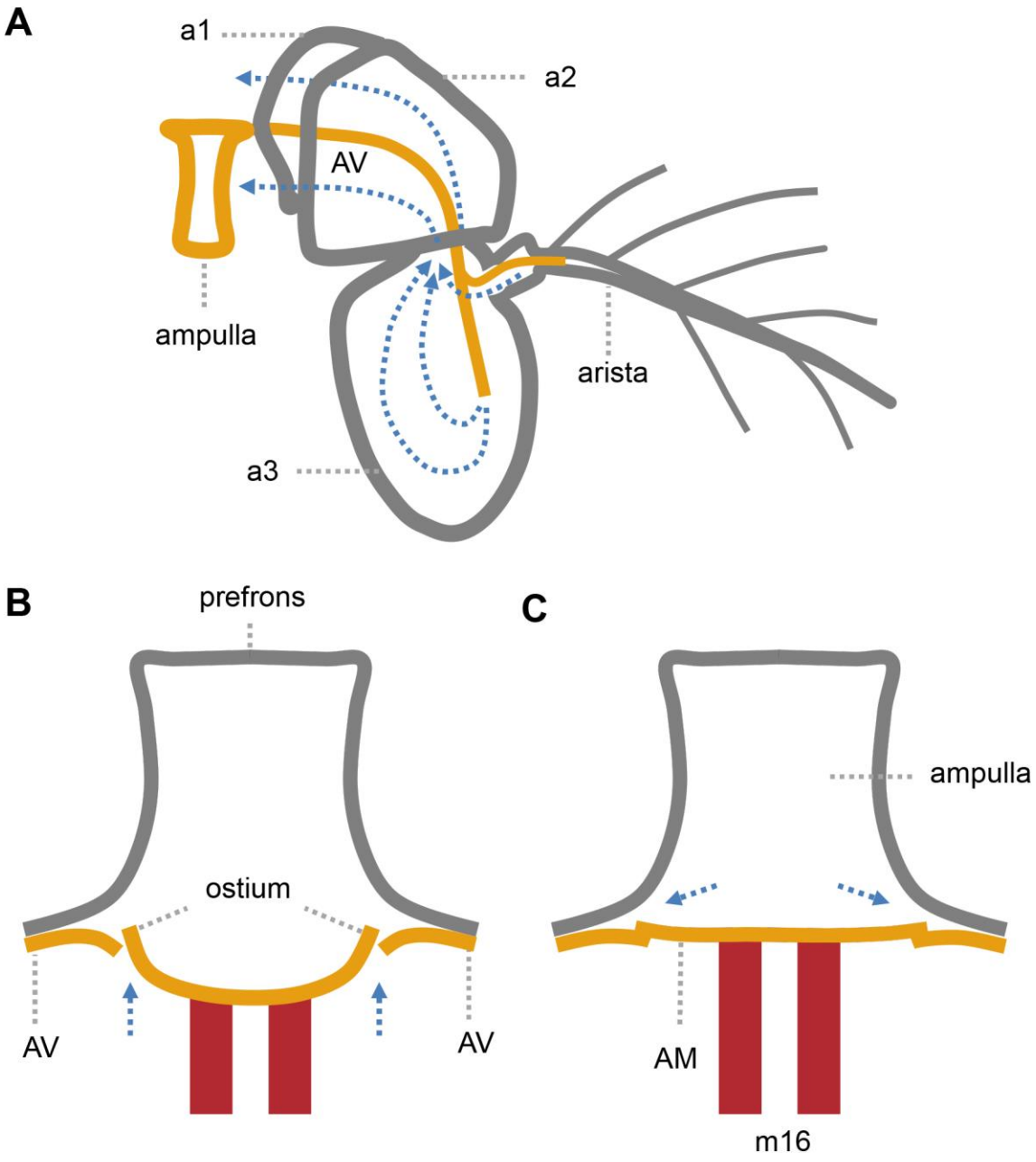

Fiig. 1. **Schematic diagram of the Drosophila antenna and FPO.** A) Frontal view of antenna and ampulla, showing the flow of hemolymph (blue arrows). Bottom, cycle of the FPO shown in a transverse section, B) active diastole C) passive systole. The ostia and m16 are probably not at the same transverse level but are depicted here as being so for simplicity.

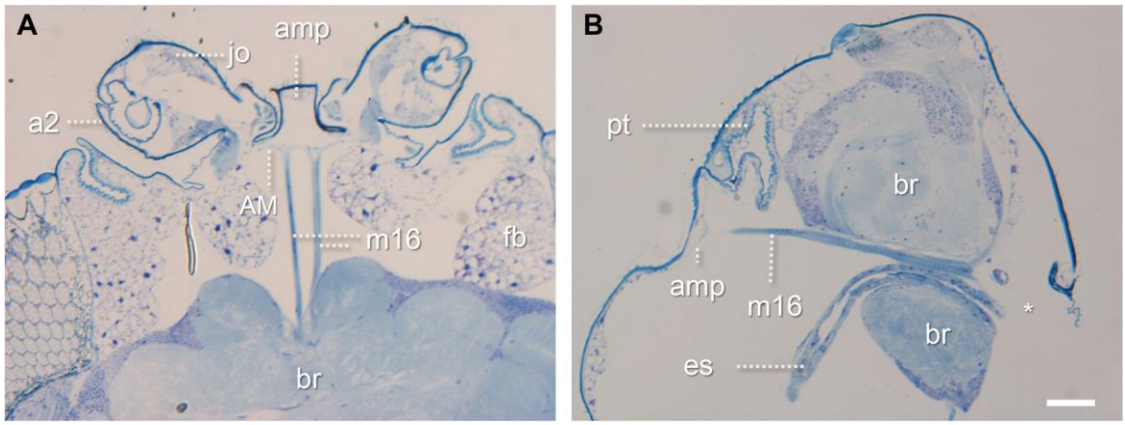

Fig. 2. Sections through *Drosophila* head showing m16 and the FPO. a) transverse and b) sagittal sections through the head. amp, ampulla; br, brain; fb, fat bodies; jo, Johnston's organ; es, esophagus; pt, ptilnum, * approximate position of the aortic funnel. Scale bar 50 μm.

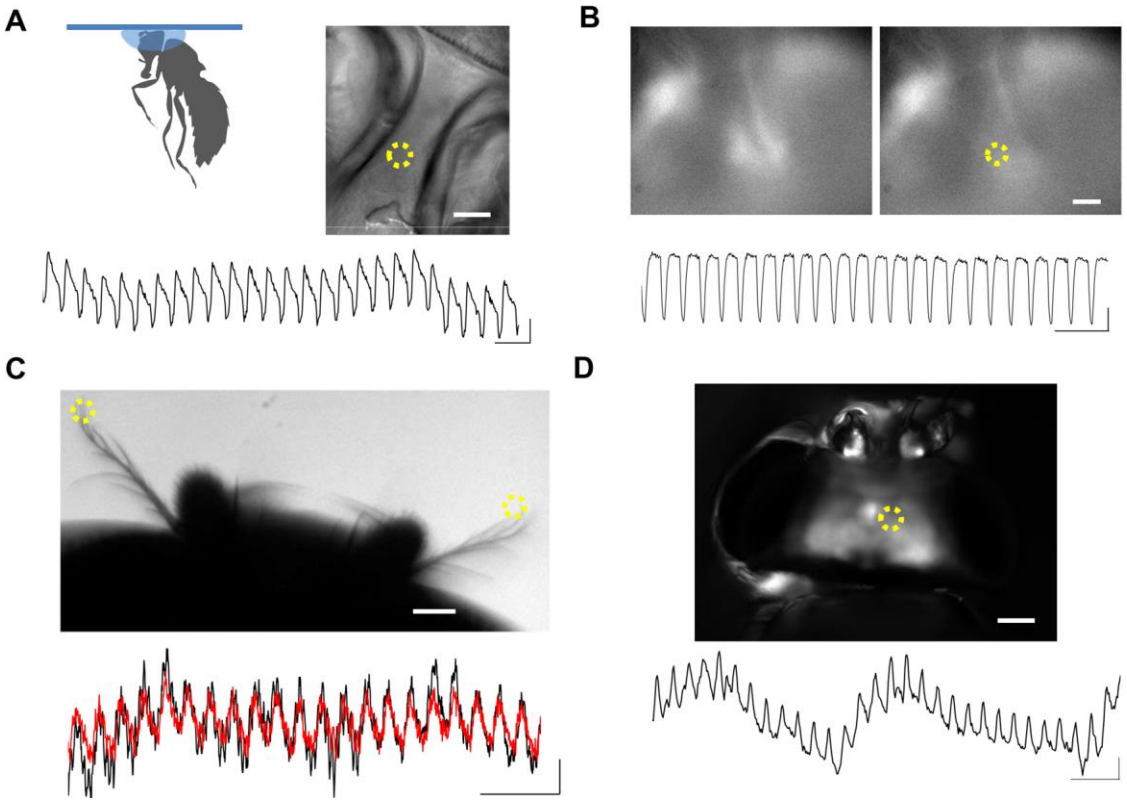

Fig. 3. Non-invasive imaging of FPO activity. A) beating of the FPO imaged through the prefrons of a fly fixed to a coverslip (inset). Trace at bottom, record of intensity fluctuation as function of time, measured in the region of interest (ROI, yellow dashed circle) in the prefrons, which is shown in the photograph (dorsal, top of image) Scale bars; 20 μm, 1% $\Delta F/F$ and 1 s. B) Activity of m16 expressing GFP (Mhc-Tau-GFP) imaged in a live fly. The vantage point is similar to that in A. Two frames of a video are shown; left peak diastole, right peak systole. The fluorescence at the top of the images is from the a1 muscles. Bottom: time-course of fluorescence in ROI. Scale bar 20um, 5% $\Delta F/F$ and 1 s . C) Synchronized bilateral vibrations of antennae. Bottom: time courses of the fluctuations of bright field light intensities in the ROIs (black, left; red, right). Scale bars, 100 μm,0.5% $\Delta F/F$ and 1 s.) D) Movement of the brain (elav-GFP) induced by FPO beating. Time course at bottom shows changes in fluctuation of fluorescent intensity in the ROI situated within the brain. Scale bars 100 μm, 0.5% $\Delta F/F$ and 1 s.

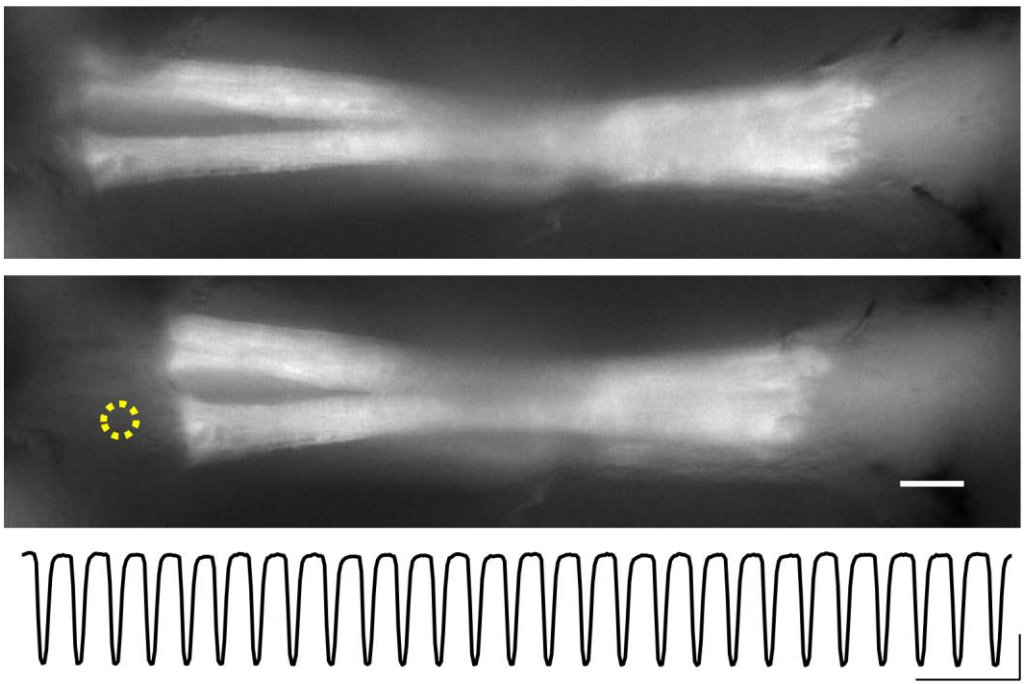

Fig. 4. Rhythmic contraction of m16 in a goggatomized *Drosophila* head. Two frames of a video are shown top, relaxed and bottom, fully contracted; anterior to the left. Trace at bottom shows the fluorescent intensity in the ROI as a function of time. Scale bars: 20 μ*m*, 10 % ΔF/F and 1 s.

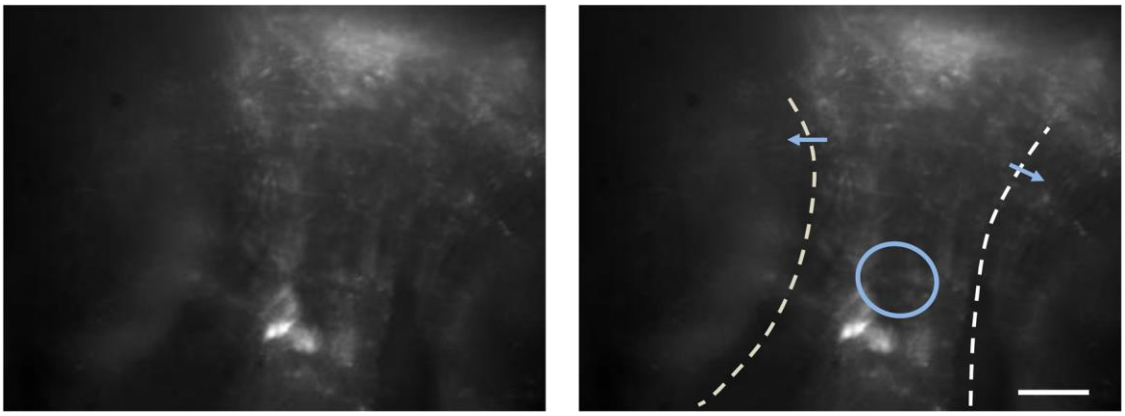

Fig. 5. Flow of beads into and out of the ampulla in control flies. The fly was mounted as in Fig. 3A, injected with beads and imaged through the prefrons. The dorsal surface is at the top of the image. The video on the left (Movie 2), with an annotated frame on the right with the following sites marked: the medial margins of a1, demarcating the edges of the ampulla (dashed white lines); approximate site (oval) where beads enter the ampulla through the ostia; AVs where beads exit the ampulla (blue arrows). Note that the AM moves in and out of the plane of focus as m16 beats. At some sites beads have become attached to the AM and ampulla. Scale bar is 20 μm. The video runs at 0.48x normal rate.

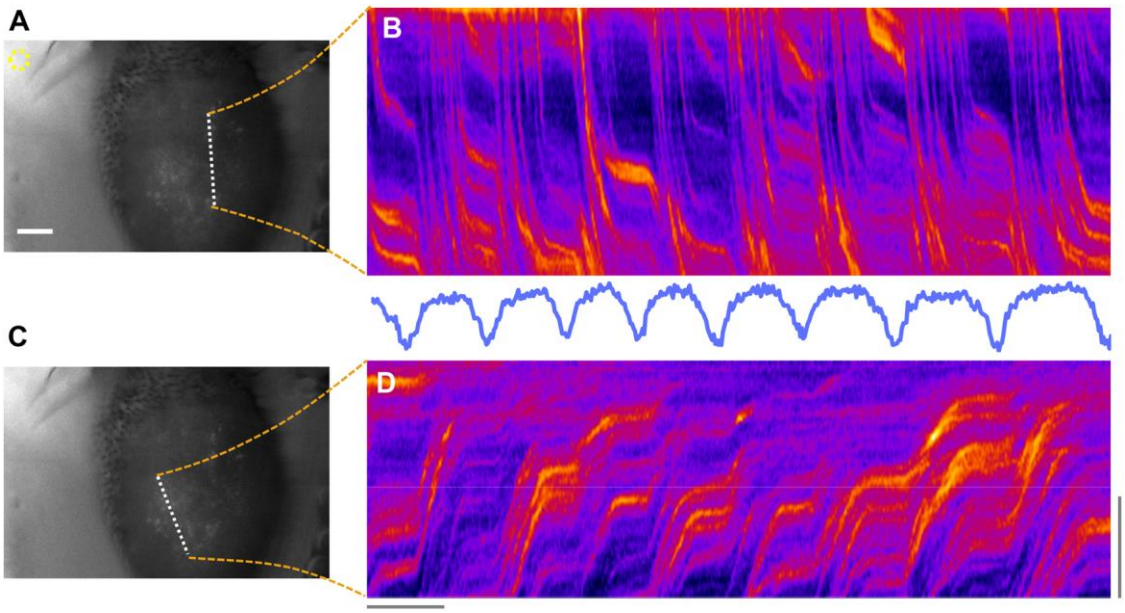

Fig. 6. Visualizing the flow rate of beads through a3 in kymograph plots. The data is derived from the video shown in Movie 3. The activity of the FPO is detected in the ROI shown in panel A (dorsal, top; ventral, bottom), which is close to the prefrons and plotted between panels B and C. The dotted white line in A overlies the AV and a kymograph of the fluorescent intensity of this line is shown in panel B. The dotted white line in panel B is used to track the flow out of a3. A kymograph of the fluorescent intensity overlying this line is shown in panel D. Note that flow is down the line in A and up the line in C. Scale bars: 20 μm, and 0.5 s.

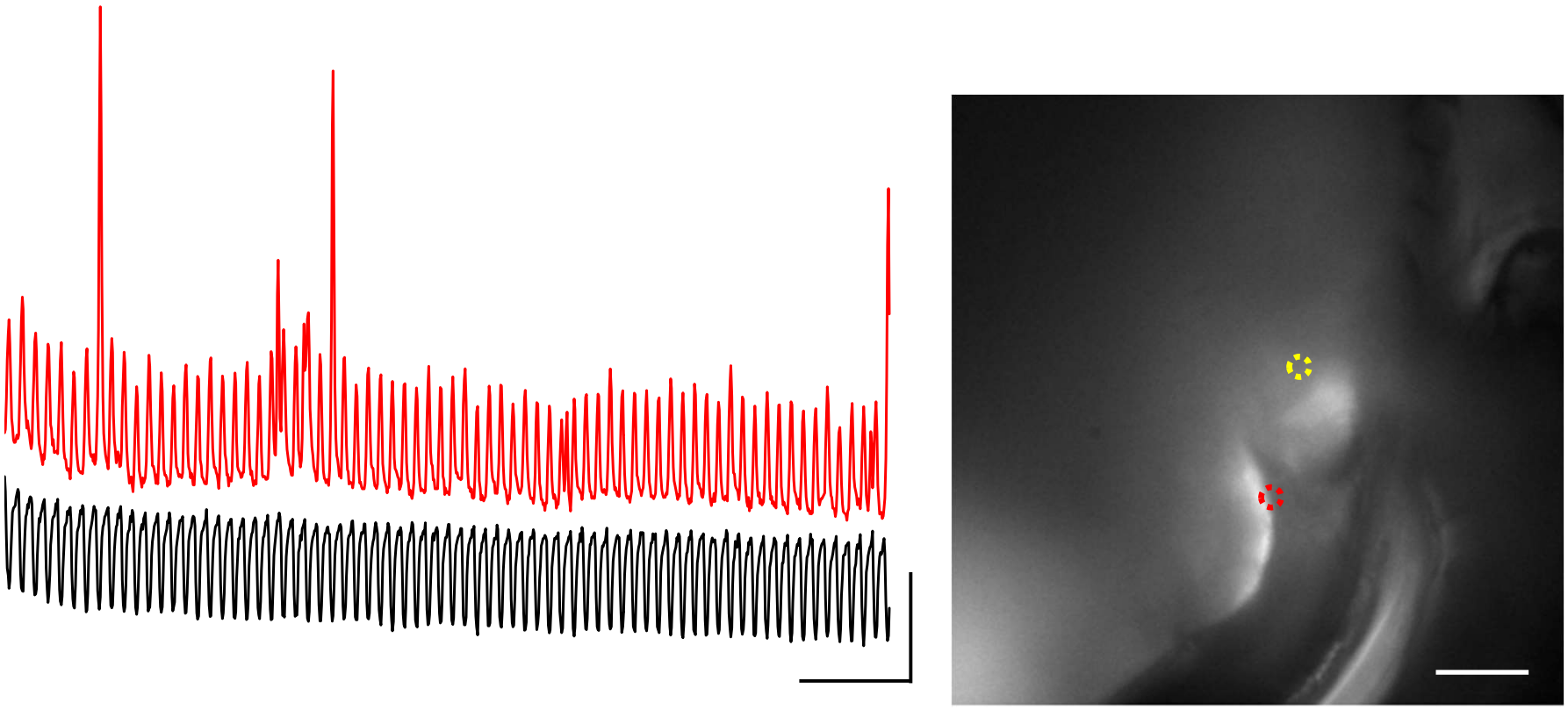

Fig. S1. Contraction of m16 rhythmically displaces the esophagus. Imaging in the head of an intact *Mhc-tau*-GFP fly. Dorsal, top of image, antenna on the right. The black trace is from the ROI (yellow) close to the ampulla, the red trace is from the ROI (red) overlying the esophagus. Scale bars, 2.5 s, 5 $\%\Delta F/F$ and 50 μm.

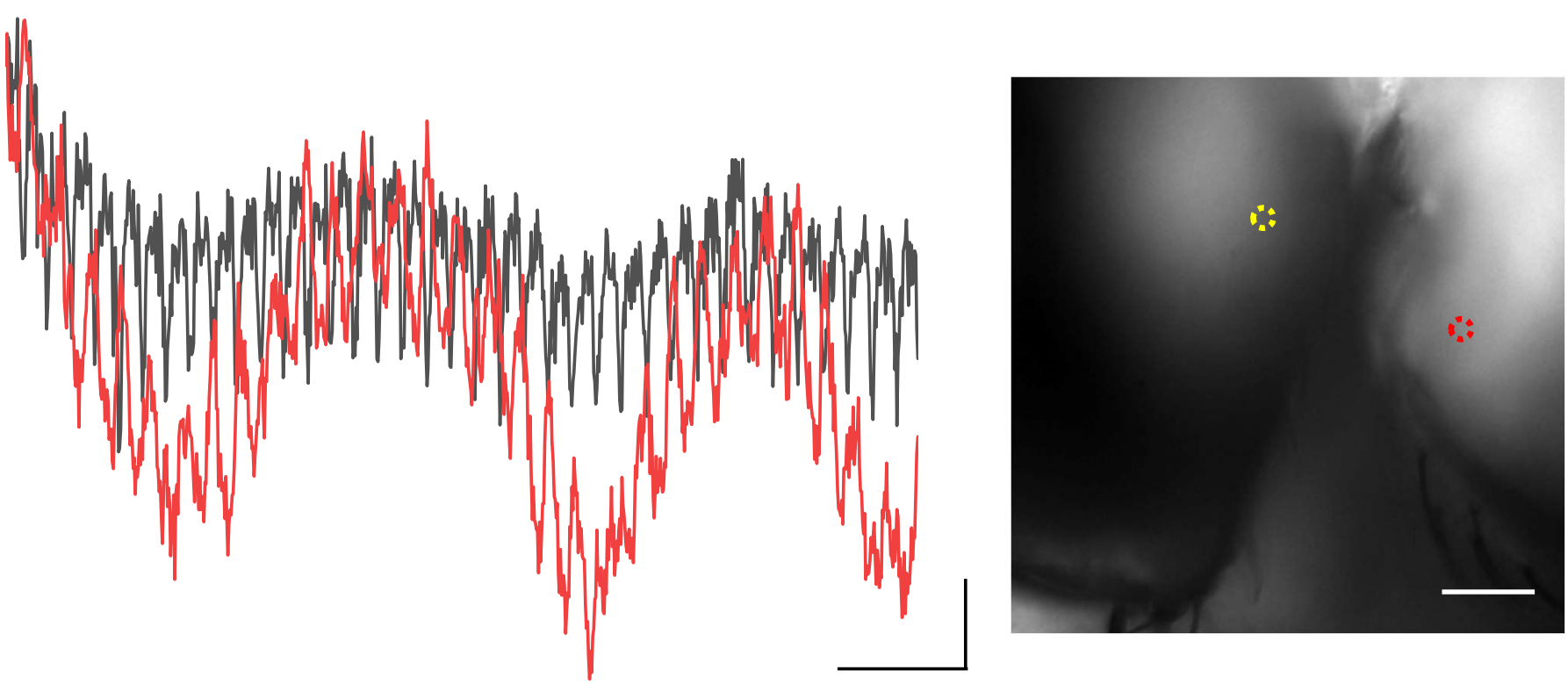

Fig. S2. Movement of the brain and ventral ganglion are independent. Imaging live elav-GFP fly. Black trace is the fluorescence intensity measured in the brain (yellow ROI), red trace ventral ganglion (red ROI), which are beating at different frequencies. Note that the slower respiratory movements are roughly synchronized in the head and thorax. Scale bars, 2.5 s, 2.5 $\%\Delta F/F$ and 50 μm.

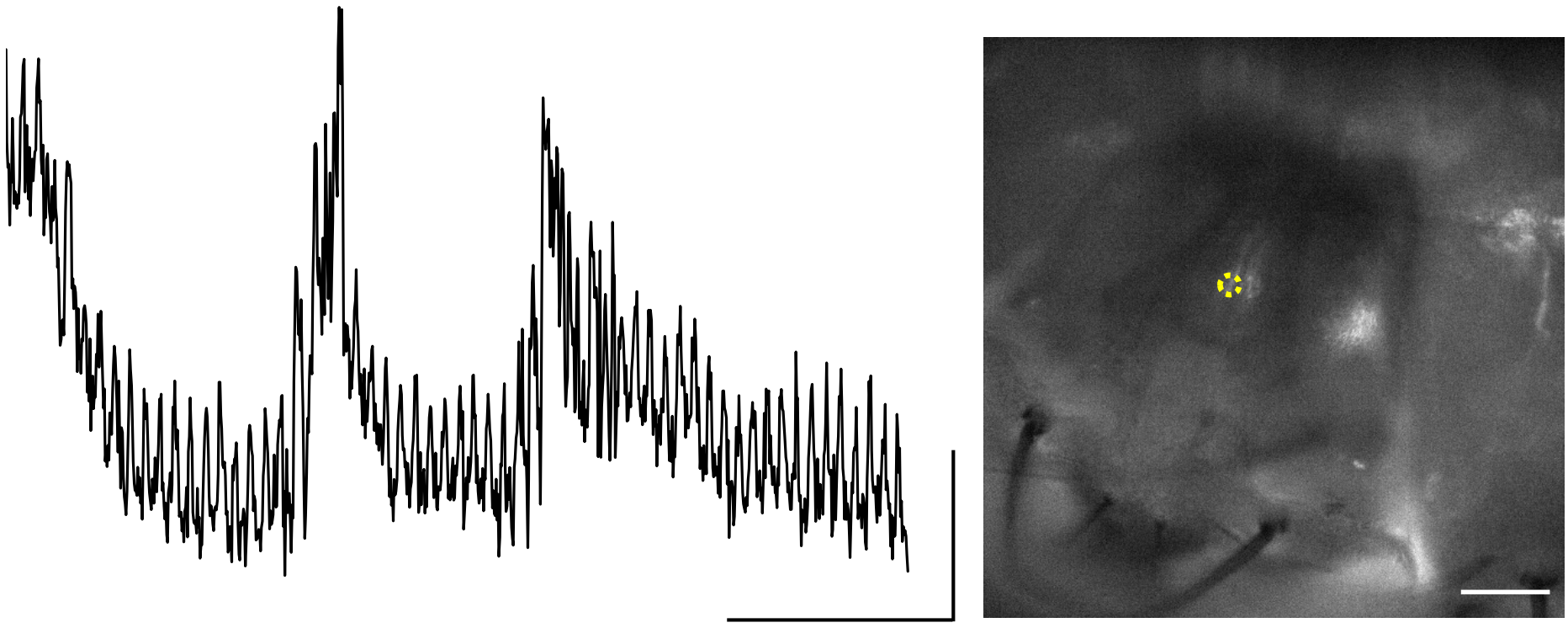

Fig. S3. Beating of m16 displaces trachea. Imaging fly expressing GFP in trachea. Change of fluorescence in the ROI in the image. View through the top of the head, with the front in the bottom left-hand corner. Scale bars, 5s, 1 $\%\Delta F/F$ and 50 μm.

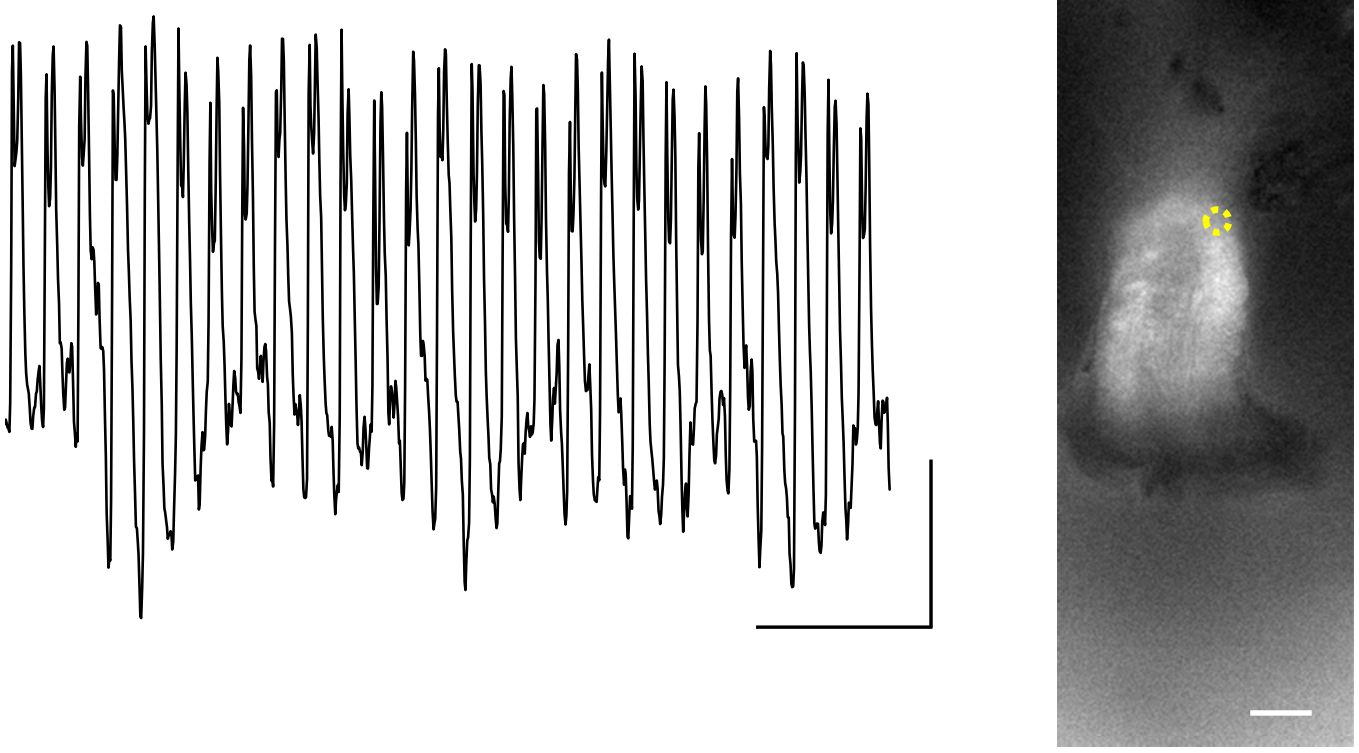

Fig. S4. Detaching m16 does not interrupt rhythmic beating. Change in fluorescent intensity in the ROI. The posterior end of m16 is at the bottom of the image. Scale bar 2s, 4 $\%\Delta F/F$ and 20 μm.

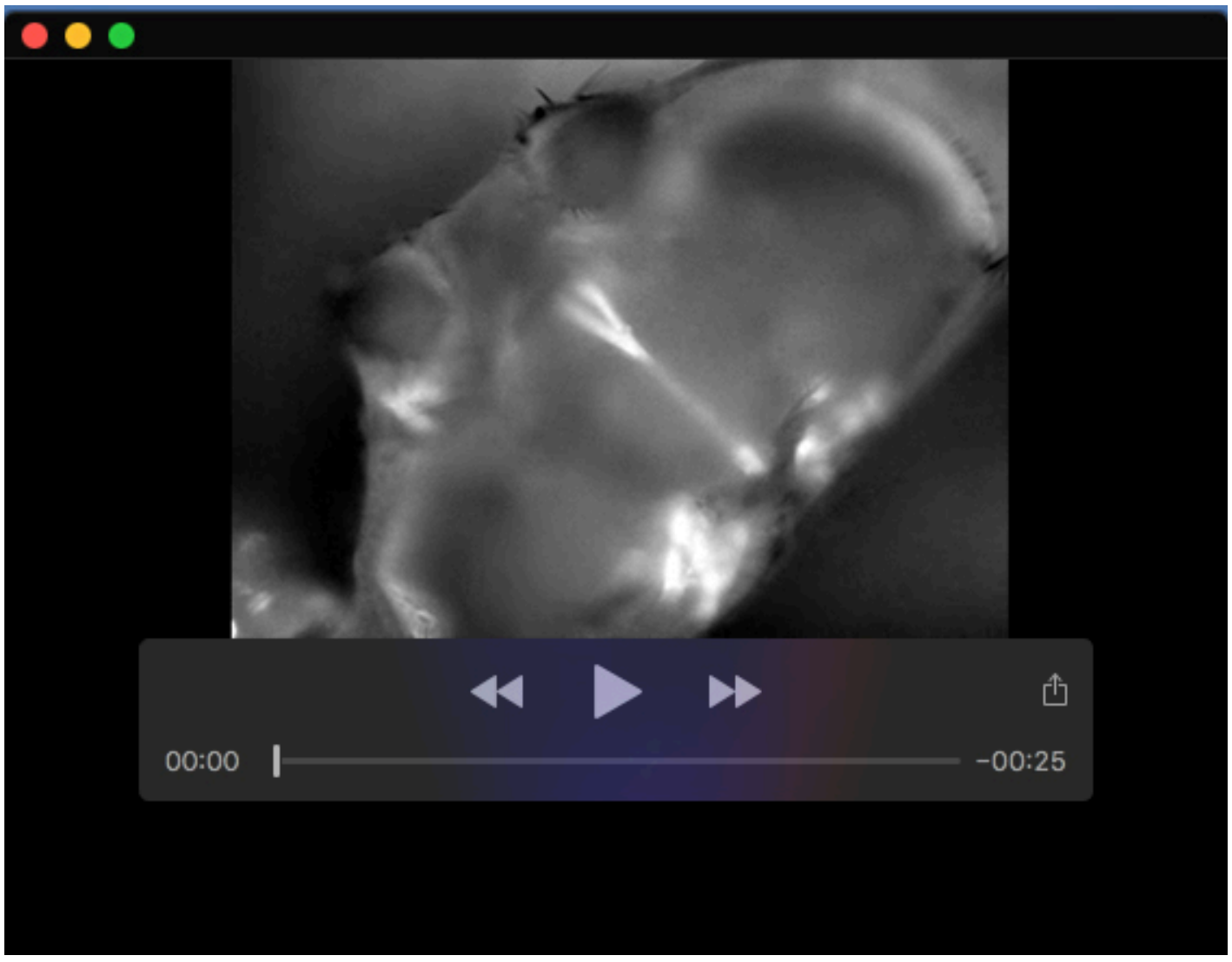

Movie 1. Beating of m16 in live transverse section of a Drosophila head. The fluorescence of m16 is diminished in areas where it is obscured by the overlying brain. The two round objects in the upper left corner are the a2s. (Mhc-Tau-GFP). The width of the image is 905 µm. The movie runs at 0.6x normal rate.

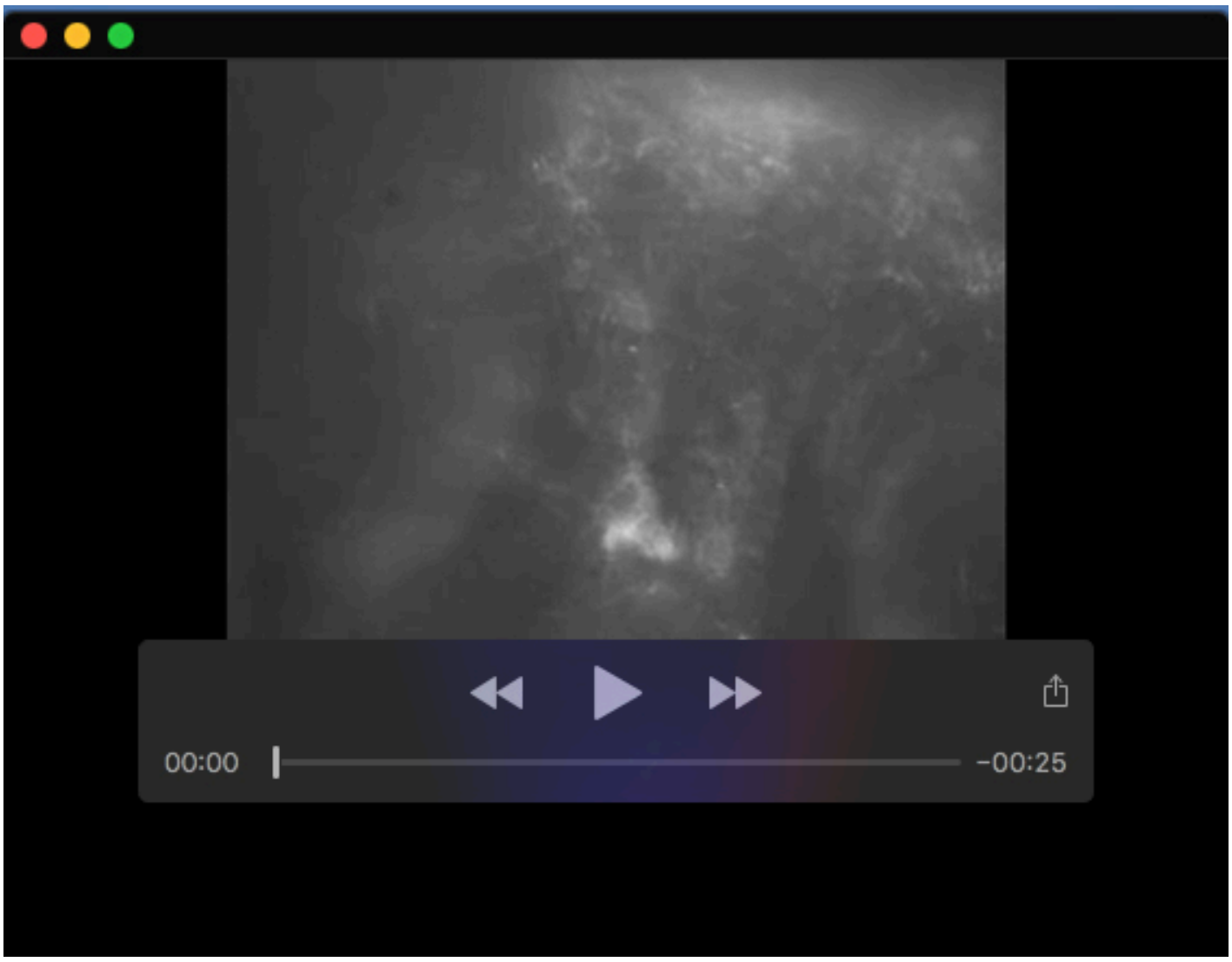

Movie 2. Flow of beads into and out of the ampulla in control flies. The fly was mounted as in Fig. 3A, injected with beads and imaged through the prefrons. The dorsal surface is at the top of the image. The video runs at 0.48x normal rate.

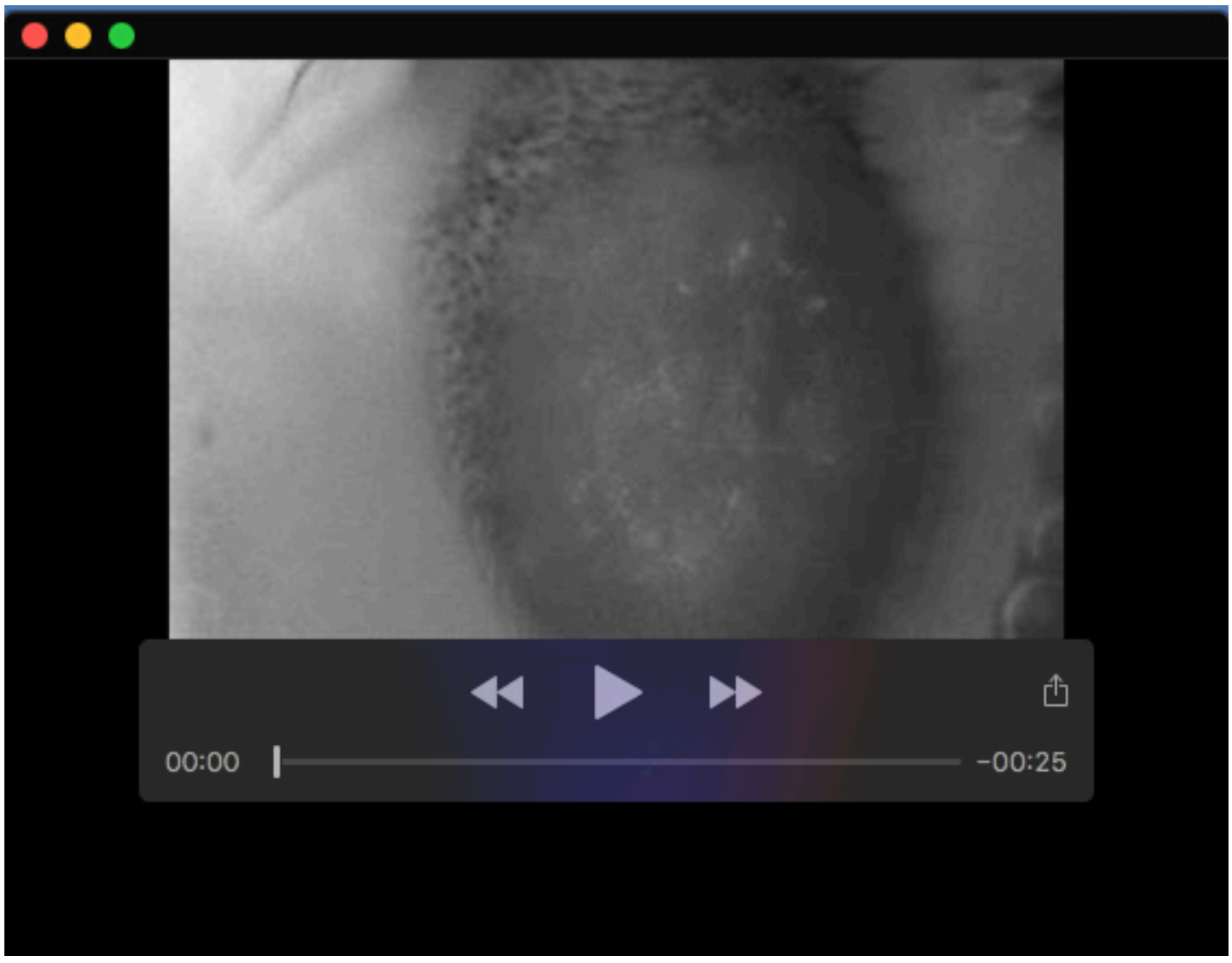

Movie 3. Beads flowing through a3. The width of the frame is 183 μm. The video runs at 0.07x normal rate.